Structuring Porous Iron-Nitrogen-Doped Carbon in a Core-Shell Geometry for Oxygen Reduction Reaction

Ming Zhou, Chunzhen Yang, and Kwong-Yu Chan*

Department of Chemistry, The University of Hong Kong, Pokfulam Road, Hong Kong
Email: hrsccky@hku.hk

The electrochemical oxygen reduction reaction (ORR) has been studied for decades in the development of fuel cells and lately for growing interests in rechargeable metal-air batteries and microbial fuel cells. The ORR is actively investigated to overcome the unresolved issues of mass-transport limitation, high costs and degradability of electrocatalysts. Non-precious metal and nitrogen doped carbons have attracted much attention for their low costs, good electrochemical activity, and durability in ORR.[1-5] The exact roles of non-precious metal and nitrogen source in providing ORR activity are under active investigations[6] while syntheses have been reported to include other precurors, such as the heteroatom(N, S, P) precursors.[7-12] With a lattice structure similar to that of graphite, nitrogen doped carbon has high crystallinity and intrinsically limited in microporosity and surface area, as shown in some examples listed in Table 1. Müllen and co-workers first reported template synthesis to introduce organized porosity in metal-nitrogen-doped carbons, achieving high surface area of ~600 m^2/g and improved ORR performance.[13]

A systematic approach to build multi-scale porosity of carbon was reported earlier in a study of electrochemical capacitance[14-16] using a hierarchical hollow core-mesoporous shell (HCMS) geometry with surface area > 1000 m^2/g and pore volume > 1.2 cm^3/g . It is desirable to use this structure to create multi-scale porosity and enhance mass transfer of ORR.

We report here for the first time, combination of the high activity of iron-nitrogen-doped carbon (Fe-N-C) and the fast transport provided by the hierarchical porosity of a uniform hollow-core mesoporous-shell (HCMS) structure. Enhanced mass transfer and durability are demonstrated in addition to the good electrochemical kinetics for oxygen reduction in acid media.

Figure 1a show a typical SEM image of the synthesized iron-nitrogen doped carbon composed of uniform discrete spheres of 600 nm averaged diameter. SEM image of the corresponding silica template is shown in **Figure S1a**. The corresponding Raman spectrum **Figure 1c** shows a typical D-band at 1330 cm^{-1} and a G-band at 1585 cm^{-1} indicating co-existence of amorphous and graphitic structures.[17-18] The corresponding XRD pattern in **Figure S2** and XPS carbon spectrum in **Figure S3(b)** also confirm both the crystalline and amorphous forms of carbon.[19] A typical EDX analysis (**Figure S4**) shows the presence of C and O, and indicates successful doping of nitrogen at 4.34% m/m. While the Fe content was too low to be quantified accurately by EDX **(Figure S4)** and TGA (**Figure S5**), it was analyzed to be 0.75% m/m by ICP-AES. The amount of iron is on the low side of previously reported values of Fe-N doped carbon,[5,6b,6c] but is crucial for ORR[5,6] by forming Fe-N$_x$ active sites and inducing favorable N-C lattice structures. The presence of Fe-N$_x$ species is shown in the XPS nitrogen spectrum of our sample **(Figure S3c)**. The absence of silicon (Si) in EDX elemental analysis confirms complete removal of the template by HF etching.[20] From the SEM and TEM images in **Figure 1**, the particles are very uniform in size with an overall diameter around 600 nm. The thickness of the porous shell is also very uniform and is measured to be 75 nm from **Figure 1b**. The core diameter of the HCMS structure is 450 nm. The synthesized carbons have highly uniform mesopores with a sharp a peak of 8 nm in the pore size distribution (**Figure 1d**), determined by nitrogen sorption analyses (**Figure S6a**). The nitrogen sorption surface area and pore volume are 1199 m^2/g and 1.77 cm^3/g,

respectively. The mesopores are arranged in random, as shown in the enlarged TEM image in Figure 1(c). From characterizations at the different length scales, the Fe-N-HCMS electrocatalyst has good integration of amorphous and crystalline lattices in a hollow core-mesoporous shell geometry and probably offers the best hierarchical structure leading to high surface area, high porosity, and mechanical robustness.

In **Figure 2**, the enhanced mass transfer of Fe-N-C in a HCMS structure is clearly demonstrated by its higher ORR diffusion limiting current when compared with a Fe-N-C carbon converted from a conventional Vulcan carbon which is without meso-structuring. The enhanced mass transfer is also evident when compared with two carbon supported Pt electrocatalysts: a commercial E-TEK Pt/C and a HCMS carbon electrode with Pt deposited (Pt-HCMS). As expected, both Pt containing catalysts have higher onset potential of ~0.9 V(RHE) and higher current densities in the activation control region of 0.60 V to 0.85 V (RHE). At potential < 0.55 V, however, the Fe-N-HCMS carbon gives higher ORR current than the two Pt catalysts. The advantage of the HCMS structure is also reflected in the better performance of Pt-HCMS with a higher diffusion limiting current compared to the randomly structured E-TEK Pt/C catalyst. In the diffusion control region, Pt-HCMS sample has lower current compared to the Fe-N-HCMS sample. While the HCMS structure is the same in both samples, only mass-transfer to locations of Pt nanoparticles can contribute to current and therefore effective diffusion is more limited. On the other hand, the Fe-N-HCMS sample has current generated throughout the structure. The ORR performance can be roughly correlated to values of surface area and pore volume which are 274 m^2/g and 0.58 mL/g for Fe-N-Vulcan versus 1199 m^2/g and 1.77 mL/g for Fe-N-HCMS, as shown in Table 1.

The mass-transfer and electrochemical performance of Fe-N-C HCMS is examined in greater details by cyclic voltammetry (CV), Koutecky-Levich analyses, rotating ring disk electrode

(RRDE) experiments, at different electrocatalysts loadings with results shown in **Figure 3(a)-(c)**. A typical CV in absence of oxygen is rectangular with no apparent peak, as shown in **Figure 3a,** indicating negligible redox reaction and inertness on the carbon surface.[5] On the other hand, the CV in presence of dissolved oxygen shows a pronounced reduction peak of -2.64 mA/cm^2 at 0.6 V. The onset potential of oxygen reduction is estimated to be 0.83 V, matching closely to other reported values[5,21] as shown in **Table 1**. Rotation dependent limiting currents at 10 mV/s linear scan are shown in **Figure 3b.** The limiting current varies from -3.8 to -7.6 mA/cm^2, when rotation increases from 400 to 2025 rpm. In Table 1, the Fe-N-HCMS sample gives at least 1 mA/cm^2 magnitude larger ORR limiting current in acid electrolyte compared to literature values of N-carbon reported at the same rotation and at the same loading.[13,21b] The rotation dependent currents of **Figure 3b** shows a linear reciprocal square-root relationship according to the Koutecky-Levich plot (inset). The intrinsic mass-transport free kinetic current (I_K) at each potential can be estimated by the y-intercepts at infinite rotation. Different electrocatlaysts are compared at a loading of 0.25 mg/cm^2. At higher loading of 0.5 mg/cm^2, the less dense Fe-N-HCMS catalyst packs into a thicker film with solid phase diffusion resistance and possible lateral diffusion as indicated by the peak currents in the polarization curves at most rotation speeds **(Figure S7a).** The polarization curve at a loading of 0.1 mg/cm^2 does not show any peak currents **(Figure S7b)** and appears to be free of thick film behavior. The different I_K values obtained from Koutecky-Levich plots at 0.6 V/RHE for different loadings in **Figure S7(c)** are proportional to mass loading except for the case of 0.1 mg/cm^2 which can be due to insufficient material for accurate measurement. The ORR current for the Fe-N-HCMS electrode at 0.25 mg/cm^2 is therefore chosen and also compared with those of other Pt containing electrocalytsts of same loading. At rotation speed of 2025 rpm, solid film and lateral diffusion effects are minimal and results at this rotation are compared in Table 1. The results show that the Fe-N-HCMS outperforms the other catalysts

when there is appreciable mass-transfer effect, as demonstrated at low rotation speeds, thick films, and potential below 0.6 V, which are all conditions of practical operation of fuel cells.

Rotating ring disk experiment indicates the number of electrons transferred to be 3.8 when potential is < 0.6 V, as shown in **Figure 3c**. This corresponds to a H_2O_2 yield of 10% suggesting that the ORR on Fe-N-HCMS carbon is mainly a four-electron process.[22] This is among the highest conversion of oxygen to water when compared to other reported values, as shown in **Table 1**, except for PANI-Fe electrocatalyst whose H_2O_2 yield is < 1% .[13] Between 0.6 ~ 0.8 V, the number of electrons transferred decreases gradually with increasing potential and has the value 3.0 at 0.8 V. As shown in **Figure S9,** a similar decrease in number of electrons transferred with higher potential is also observed in the Tafel plot of the kinetic currents obtained from the Koutecky-Levich plot. The kinetic currents are derived from linear scan voltammetry which is independent of RRDE experiments.

An inherent disadvantage of Pt electrocatalyst is its vulnerability to methanol or other fuels that easily crossover in a direct liquid fuel cell. The Fe-N-HCMS electrocatalyst shows excellent tolerance to methanol with indistinguishable ORR performance with or without methanol. As shown in **Figure 4(a)**, this contrasts with the ORR currents of Pt containing electrocatalysts which are positive above 0.6 V, indicating oxidation of methanol due to high anodic activity of Pt. Durability of electrocatalysts is another obstacle to commercialization of fuel cells and metal-air batteries. Materials are vulnerable to corrosion in air cathodes since they operate at high potential in an oxygen environment. In lieu of Pt nanoparticles, nitrogen doped carbon with increased graphite-type lattice has good stability.[23] Durability of the synthesized Fe-N-HCMS carbon is examined by accelerated degradation tests[5] (ADT) with cycling between 0.6 and 1.0 V (RHE) at 10 mV/s. Linear scan voltammetry in saturated oxygen is performed after subjecting the electrocatalysts to ADT cycling. As observed in **Figure 4(b)**, the oxygen reduction curve has less than 20 mV loss in oxygen reduction potential after 1000 cycles of ADT. This value is much lower than most reported values in

acid environment.[12] The normalized loss of potential at -2.5 mA/cm^2, at the end of 1000 cycle, expressed as $(E_{initial}-E_{1000})/E_{initial}$ x 100%, is used to quantify the comparison among the tested electrocatalysts, as shown in the inset of **Figure 4(b)**. The Fe-N-HCMS electrocatalyst demonstrates excellent durability with less than 3% loss of activity. This high stability can be attributed to the inertness of the carbon surface, in absence of functional groups or metal/metal oxide redox species, as indicated in the featureless rectangular CV of **Figure 3a**. On the other hand, the two supported Pt nanoparticle catalysts suffer serious potential loss of > 35% for E-TEK Pt/C and > 25% for Pt-HCMS, probably due to the loss and de-activation of Pt nanoparticles.[23] Among the two Pt containing catalysts, Pt-HCMS shows higher durability compared to that of E-TEK and can be attributed to better dispersion and protection of Pt nanoparticles by the regular mesopores of the HCMS structure.[24]

In summary, the synthesized Fe-N-HCMS carbon demonstrates superior ORR performance among different non-precious electrocatalysts. It has a high onset potential of 0.83 V (vs RHE), a high limiting current density of -7.6 mA/cm^2 at 2025 rpm, high tolerance to methanol and high stability with < 4% loss of reduction potential at -2.5 mA/cm^2 after 1000 cycles of accelerated degradation test.

As determined by ring-disk-electrode experiments, conversion of oxygen to water is almost complete with 3.8 electrons transferred except closed to OCP where a two-electron ORR reaction is observed. The excellent performance indicators can be attributed to integration of the partially crystalline lattice of Fe-N-C into a regular hollow core mesoporous shell structure, leading to enhanced mass-transfer, high surface area for charge transfer, mechanical strength, and resistance to degradation. Extension of the Fe-N-HCMS electrocatalyst to ORR in non-aqueous solutions and in Li-Air batteries are promising and will be the focus of future work.

Experimental Section

Preparation of iron-nitrogen-doped hollow core mesoporous shell carbon

Typically, 0.1 g $Fe(NO_3)_3 \cdot 9H_2O$ was dissolved in 0.5 ml ethylenediamine (EDA) via ultrasonification for 30 min and then mixed with 0.5 ml furfuryl alcohol (FA). The mixed solution was dropped onto a mortar containing 1 g silica template and the mixture grinded to complete impregnation. FA and iron source impreganated silica was heated at 80 ℃ for 3 h and then 160 ℃ for 3 h in air. Carbonization was performed in a tube furnace at 900 ℃ in argon atmosphere for 1 h. After cooling, soluble iron species and the silica template were removed by immersion in 10 wt% hydrofluoric acid (HF) solution. The silica-free carbon material was washed with 1:1 water/ethanol solution and then calcinated at 900℃ in argon atmosphere for 3 h. The as-synthesized material was denoted as Fe-N-HCMS carbon.

Characterization

Transition electron microscopy (TEM, Philips TECNAI 20 at 200 kV) and field emission scanning electron microscopy (SEM, Hitachi S-4800) were used to characterize the morphologies of the synthesized materials. Energy-dispersive X-ray spectroscopy (EDX) was performed on the SEM equipped with INCAx-sight EDX detectors (Oxford Instruments). Nitrogen sorption isotherms were obtained on a Micromeritics ASAP 2020 analyzer at 77 K. The specific surface area was determined using the Brunauer-Emmett-Teller (BET) method. The pore size distribution was derived from the desorption branch using Barrett-Joyner-Halenda (BJH) method. Powder X-ray diffraction (XRD) patterns were collected on a PANalytical X-ray diffractometer using Cu Kα radiation ($\lambda = 0.1541$ nm) at a sweep rate of 0.02 deg/s. The Raman spectrum was obtained on Renishaw Invia Raman microscope

(Renishaw, UK) equipped with a He-Ne laser (633 nm, 25 mW). For ICP-AES experiments, electrocatalyst sample was prepared by digesting 0.03 g Fe-N-HCMS in 50 ml 2 wt% HNO_3 and dilute the solution to obtain appropraite Fe ion concentration at ppm level for analysis. The Fe concentration is determined to be 4.5 ppm against pre-calibrated standards, corresponds to 0.75% m/m the Fe-N-HCMS sample.

Electrochemical measurements

Electrochemical measurements were conducted on a Solatron SI1287 potentiostat and Biologic multi-channel electrochemical station. A three-electrode configuration with Pt wire counter electrode, Hg/Hg_2SO_4 reference electrode, and a working electrode of 5.0 mm diameter glassy carbon (GC) rotating disk electrode (RDE) was used. In the rotating ring disk electrode (RRDE) experiments, the working electrode was a 5.61 mm GC disk electrode and a Pt ring electrode (inner diameter: 6.25 mm; outer diameter: 7.92 mm; collection efficiency N= 0.37). A Princeton Applied Research model 636 electrode rotator was used for RDE and a multichannel Biologic potentiostat was used for the RRDE measurements. All recorded potentials were converted to the scale of reversible hydrogen electrode (RHE). The ORR activity were determined in 0.5 M H_2SO_4 at room temperature (~23 ℃) with 0.5 mg/cm^2 catalyst loading. Pt containing samples were tested in 0.1 M $HClO_4$ solution using a Ag/AgCl reference electrode in 3.0 M KCl.[5] The first is a commerical E-TEK 10 wt% Pt on Vulcan carbon. The second is 10 wt% Pt loaded on hollow core mesoporous shell carbon (HCMS) without iron or nitrogen doping and prepared using a previous procedure of carbonization over protected and dispersed metal (CPDM).[24] Each catalyst ink was prepared by mixing 5 mg catalyst with 0.5 ml isopropanol alcohol, 0.5 ml DI water, and 20 μl 0.5 wt% Nafion solution. Then, 20 μl of the ink was deposited onto the glassy carbon and dried at room temperature. To maintain the same catalyst loading per unit area, 24 μl catalyst ink was used

in the RRDE tests. For other loadings, the proportional volume of catalyst ink was dropped

onto the glassy carbon rotating electrode. The ORR current densities were determined through

linear scan voltammetry in oxygen saturated electrolytes from 0.0 to 1.0 V at 10 mV/s. The

disk electrode was rotated at 400 to 2025 rpm. Accelerated durability tests were conducted in

nitrogen-saturated electrolytes using cyclic voltage scanning between 0.6 and 1.0 V at 10

mV/s.

Supporting Information

The synthesis, characterization, morphology, and porosity of silica template used in this article. XRD pattern, nitrogen sorption isotherm and Tafel plot for Fe-N-HCMS are available online from the Wiley Online Library.

Acknowledgements

Received: ((will be filled in by the editorial staff))
Revised: ((will be filled in by the editorial staff))
Published online: ((will be filled in by the editorial staff))

[1] J. S. Lee, S. T. Kim, R. Cao, N. S. Choi, M. Liu, K. T. Lee, J. Cho, *Adv. Energy Mater.* **2011**, *1*, 34.

[2] R.Cao, J. S. Lee, M. Liu, J. Cho, *Adv. Energy Mater.* **2012**, *2*, 816.

[3] J. S. Lee, G. S. Park, S. T. Kim, M. Liu, J. Cho, *Angew. Chem. Int. Ed.* **2013**, *52*, 1026.

[4] B. Cao, G. M. Veith, R. E. Diaz, J. Liu, E. A. Stach, R. R. Adzic, P. G. Khalifah, *Angew. Chem. Int. Ed.* **2013**, *52*, 10753.

[5] G. Wu, K. L. More, C. M. Johnston, P. Zelenay, *Science*, **2011**, *332*, 443.

[6] (a) Y. Y. Shao, J. H. Sui, G. P. Yin, Y. Z. Gao, *Appl. Catal. B* **2008**, *79*, 89; (b) S. Zhang, H. Zhang, Q. Lin, S. Chen, *J. Mater. Chem. A,* **2013**, *1*, 3302; (c) M. Ferrandon, AJ Kropf, DJ Myers, K Artyushkova, U Kramm, P. Bogdanoff, G. Wu, C.M. Johnston, and P. Zelenay, *J. Phys. Chem. C,* **2012**, *116*, 16001.

[7] I. Y. Jeon, S. Zhang, L. Zhang, H. J. Choi, J. M. Seo, Z. Xia, L. Dai, J. B. Baek, *Adv. Mater.* **2013**, *25*, 6138.

[8] S. Yang, L. Zhi, K. Tang, X. Feng, J. Maier, K. Müllen, *Adv. Funct. Mater.* **2012**, *22*, 3634.

[9] Z. W. Liu, F. Peng, H. J. Wang, H. Yu, W. X. Zheng, J. Yang, *Angew. Chem. Int. Ed.* **2011**, *50*, 3257.

[10] P. H. Matter, L. Zhang, U. S. Ozkan, *J. Catal.* **2006**, *239*, 83.

[11] a) Y. Tan, C. Xu, G. Chen, X. Fang, N. Zheng, Q. Xie, *Adv. Funct. Mater.* **2012**, *22*, 4584; b) Y. Zheng, Y. Jiao, M. Jaroniec, Y. Jin, S. Z. Qiao, *Small*, **2012**, *8*, 3550; c) E. J. Biddinger, D. Von Deak, U. S. Ozkan, *Top. Catal.* **2009**, *52*, 1566.

[12] F. Jaouen, E. Proietti, M. Lefèvre, R. Chenitz, J. P. Dodelet, G. Wu, H. T. Chung, C. M. Johnston, P. Zelenay, *Energy Environ. Sci.* **2011**, *4*, 114.

[13] a) R. Liu, D. Wu, X. Feng, K. Müllen, *Angew. Chem.* **2010**, *122*, 2619; b) H. W. Liang, W. Wei, Z. S.Wu, X. Feng, K. Müllen, *J. Am. Chem. Soc.* **2013**, *135*, 16002.

[14] F. Li, M. Morris, K. Y. Chan, *J. Mater. Chem.* **2011**, *21*, 8880.

[15] S. B. Yoon, J. Y. Kim, J. H. Kim, Y. J. Park, K. R. Yoon, S. K. Park, J. S. Yu, *J. Mater. Chem.* **2007**, *17*, 1758.

[16] J. H. Kim, S. B. Yoon, J. Y. Kim, Y. B. Chae, J. S. Yu, *Colloids Surf. A* **2008**, *313-314*, 77.

[18] a) M. A. Pimenta, G. Dresselhaus, M. S. Dresselhaus, L. G. Cancado, A. Jorio, R. Saito, *Phys. Chem. Chem. Phys.* **2007**, *9*, 1276; b) S. C. Ray, Z. N. Tetana, R. Erasmus, Ashish Mathur, N. J. Coville, *Int. J. Energy Res.* **2013**, DOI: 10.1002/er.3079.

[19] H. Shi, J. Barker, M. Y. Saïdi, R. Koksbang, L. Morris, *J. Power Sources* **1997**, *68*, 291.

[20] S. Jun, S. H. Joo, R. Ryoo, M. Kruk, M. Jaroniec, Z. Liu, T. Ohsuna, O. Terasaki, *J. Am. Chem. Soc.* **2000**, *122*, 10712.

[21] a) H. L. Jiang, B. Liu, Y. Q. Lan, K. Kuratani, T. Akita, H. Shioyama, F. Zong, Q. Xu, *J. Am. Chem. Soc.* **2011**, *133*, 11854; b) T. Palaniselvam, B. P. Biswal, R. Banerjee, S. Kurungot, *Chem. Eur. J.* **2013**, *19*, 9335.

[22] a) J. Zhang, Y. Mo, M. B. Vukmirovic, R. Klie, K. Sasaki, R. R. Adzic, *J. Phys. Chem. B* **2004**, *108*, 10955; b) N. A. Vante, *Chem. Phys. Chem.* **2010**, *11*, 2732.

[23] P. J. Ferreira, G. J. La Ọ, Y. Shao-Horn, D. Morgan, R. Makharia, S. Kocha, H. A. Gasteiger, *J. Electrochem. Soc.* **2005**, *152*, A2256.

[24] F. Li, K. Y. Chan, H. Yung, *J. Mater. Chem.* **2011**, *21*, 12139.

[25] a) W. Chen, S. W. Chen, *Angew. Chem.* **2009**, *121*, 4450; b) W. Chen, S. W. Chen, *Angew. Chem. Int. Ed.* **2009**, *48*, 4386.
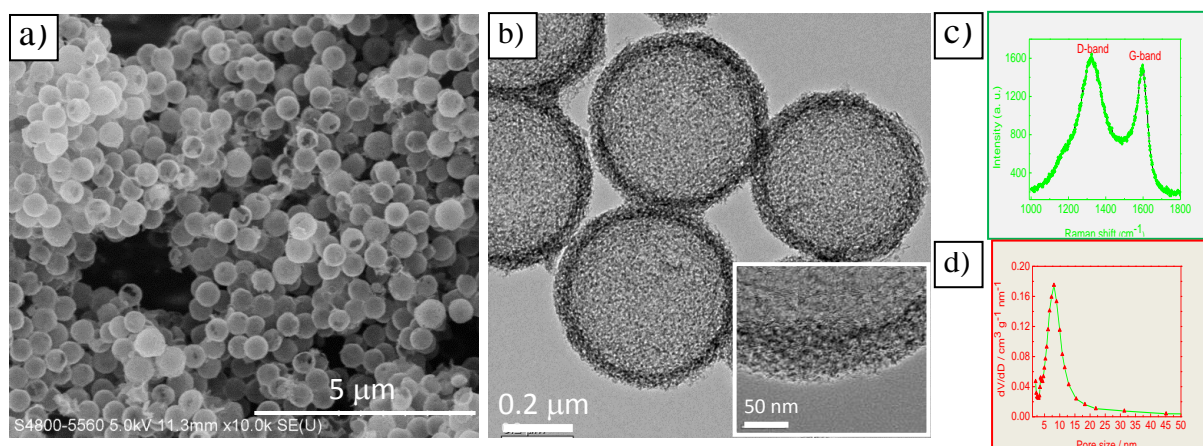
Figure 1. (a) SEM image, (b) TEM image with inset showing a shell region at higher resolution, (c) Raman Spectrum, and (d) nitrogen sorption pore size distribution, of the synthesized Fe-N-HCMS.
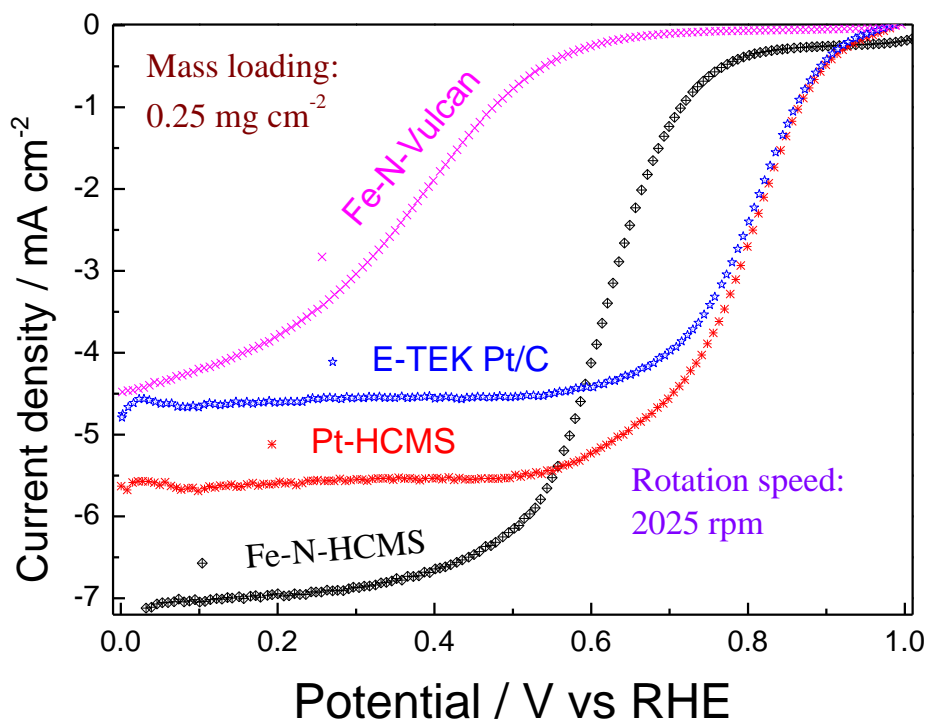
Figure 2. Linear scan voltammetry at 10 mV/s of electrodes with separate 0.25 mg/cm^2 loadings of Fe-N-HCMS, E-TEK Pt/C, Pt-HCMS, and Fe-N-Vulcan with rotation at 2025 rpm in 0.5 M H_2SO_4 electrolyte saturated with oxygen. (Surface areas of the samples are 1199, 154, 1072, and 274 m^2/g and pore volumes are 1.77, 0.37, 0.81, and 0.58 mL/g, respective to their order above.)
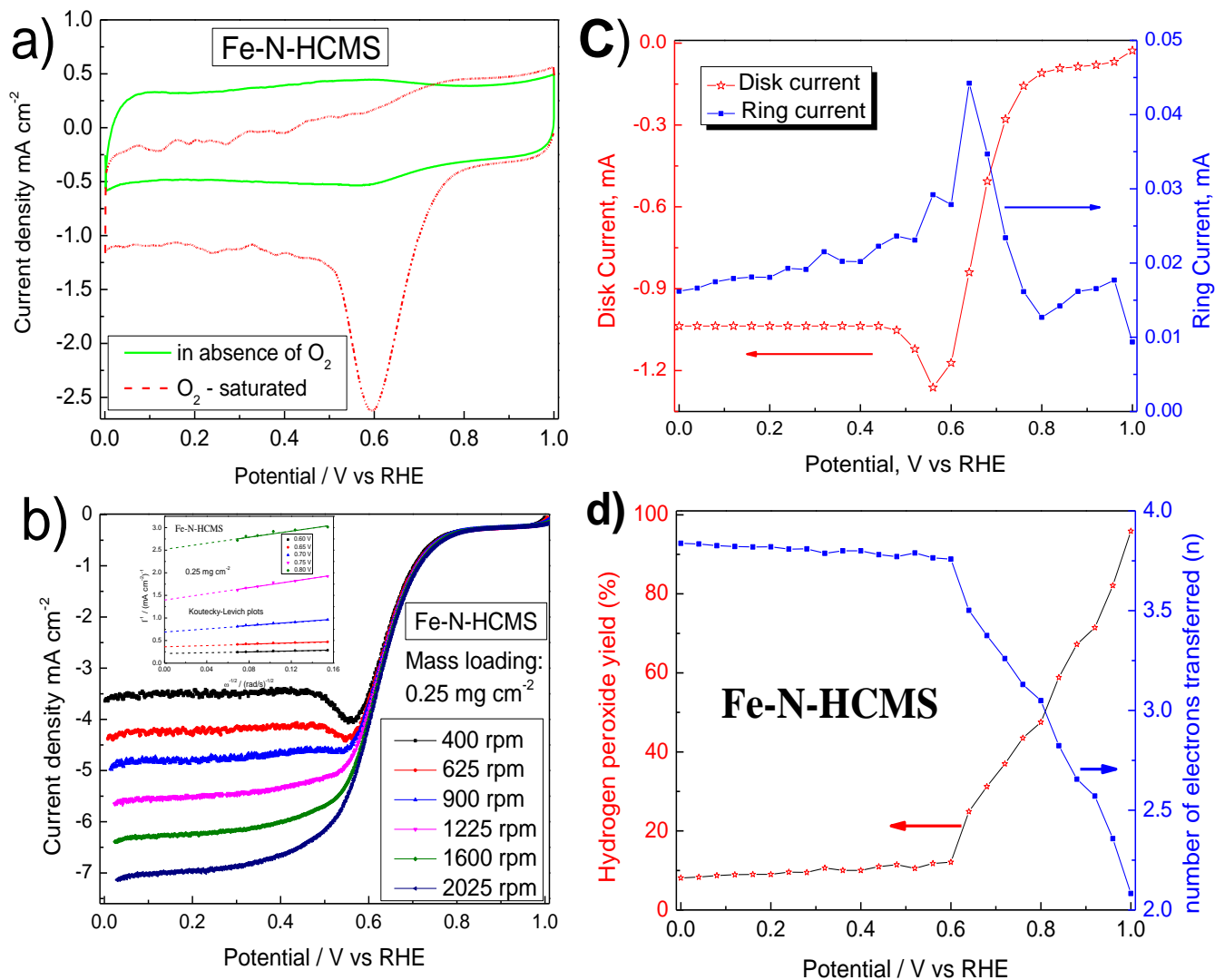
Figure 3. (a) CV at scan rate of 10 mV/s for 0.5 mg/cm^2 Fe-N-HCMS in 0.5 M H$_2$SO$_4$ with and without saturated O$_2$; (b) linear scan voltammetry at 10 mV/s for 0.25 mg/cm^2 Fe-N-HCMS carbon particles in presence of oxygen with rotation speed from 400 to 2025 rpm and the corresponding Koutecky-Levich plots in the inset; (c) Ring and disk currents obtained in presence of oxygen and with rotation speed of 900 rpm using mass loading of 0.5 mg/cm^2; (d) corresponding number of electrons transferred and hydrogen peroxide yield determined from rotating ring-disk electrode results in (c).
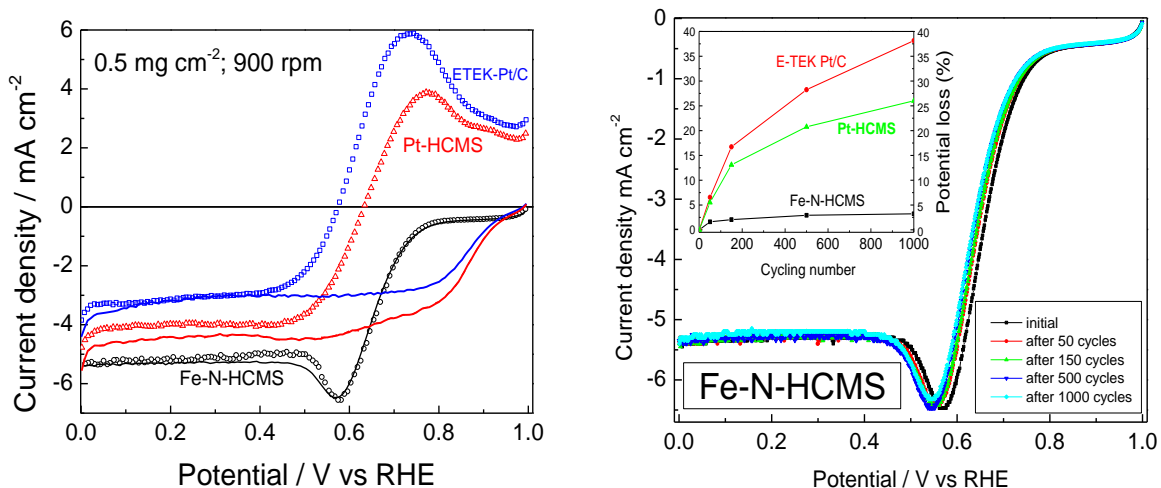
Figure 4.(a) Tolerance of ORR to methanol present in 1 mL per 50 mL 0.5 M H_2SO_4 with rotation speed of 900 rpm using mass loading of 0.5 mg/cm². The open squares, triangles, and circles are ETEK, Pt-HCMS, and Fe-N-HCMS, respectively. The lines in corresponding color and order are ORR curves in absence of methanol.

b) linear scan voltammetry at 10 mV/s and 900 rpm for a 0.5 mg/cm2 Fe-N-HCMS subjected to cylcing between 0.6 and 1.0 V at 10 mV/s; Inset shows the corresponding percentage potential loss [($E_{initial} - E_{1000}$)/$E_{initial}$] x100% at 2.5 mA/cm² after 1000 cycles, compared with Pt electrocatalysts.

Table 1 Electrochemical performance of different electrocatalysts for oxygen reduction reaction.

(a) Performance tested in 0.1 M KOH

Sample	Surface area	Pore volume	Loading	Onset potential (V vs RHE)	Current at 0.6 V vs RHE	Limiting current (mA/cm^2)	Number of Electrons Transferred (n)	H_2O_2 yield (%)	Ref.
	m^2/ g	mL/ g	mg/cm^2						
Ketjenblack EC-600	---			0.18 (alkaline)		6.5 @ 2000 rpm	3.85	15	3
P-doped graphite	0.399			0.1 (alkaline)		4.3 @ 1100 rpm	3	---	9

(b) Performance tested in 0.5 M H$_2$SO$_4$

Sample	Surface area	Pore volume	Loading	Onset potential (V vs RHE)	Current at 0.6 V vs RHE	Limiting current (mA/cm^2)	Number of Electrons Transferred (n)	H_2O_2 yield (%)	Ref.
	m^2/ g	mL/ g	mg/cm^2						
PANI-Fe	568		0.6	0.85@10mV/s		4.5 @ 1600 rpm	3.95[§]	0.71[§]	13b
*FeNC-70	262		0.25	0.8@10mV/s		4 @ 1600 rpm	3.5	---	21b
Fe-N-HCMS	1199	1.77	0.5 / 0.25	0.80@10mV/s	5.5 / 4.13	6.8 @ 1600 rpm / 6.3 @ 1600 rpm / 7.0 @ 2025 rpm	3.8[#]	12[#]	This work
Fe-N-Vulcan	274	0.58	0.25	0.55@10mV/s	0.30	4.5 @ 2025 rpm			This work
E-TEK Pt/C	154	0.37	0.25	0.92@10mV/s	4.41	4.6 @ 2025 rpm			This work
Pt-HCMS	1072	0.81	0.25	0.92@10mV/s	5.21	5.6 @ 2025 rpm			This work

[§]determined at 0.7 V vs RHE, *tested in 0.5 M HClO$_4$
[#]determined at 0.6 V vs RHE.

Highly porous iron-nitrogen doped hollow core mesoporous shell (Fe-N-HCMS) carbon is synthesized with regular mesopores attributing to high surface area and large pore volume. Excellent mass transfer, durability, methanol tolerance, and high activity for oxygen reduction reaction are shown and the limiting current densities is the highest among the published results of non-precious metal-nitrogen-doped carbons.

Keywords: hierarchical porous structure, iron-nitrogen-doped carbon, oxygen reduction reaction, metal-air batteries, fuel cells

Ming Zhou, Chunzhen Yang, and Kwong-Yu Chan*

Structuring Porous Iron-Nitrogen-Doped Carbon in a Core-Shell Geometry for Oxygen Reduction Reaction

Table of Contents